TASK QUARTERLY 7 No 3 (2003), 425–438

INFLUENCE OF VISCOSITY DIFFERENCE ON THE INSTABILITY OF THE CORE-ANNULAR FLOW

ANTONI ROŻEŃ AND JERZY BAŁDYGA

Department of Chemical and Process Engineering,
Warsaw University of Technology,
Waryńskiego 1, 00-645 Warsaw, Poland
{rozen,baldyga}@ichip.pw.edu.pl

(Received 9 December 2002)

Abstract: The process of destabilisation of an axi-symmetric, core-annular flow (CAF) of two Newtonian fully miscible liquids widely differing in viscosity is investigated. Formation of periodic structures is observed in experiments, predicted by the linear stability theory and simulated numerically using the volume of fluid method (VOF). Possible influence of this phenomenon on mixing on the molecular scale is discussed.

Keywords: laminar flow, micromixing, stability analysis, viscous liquids

Notation

a_i – length of semi-axes of an ellipsoidal inclusion [m],
c – imaginary wave speed [m·s^{-1}],
F – volume marker concentration [–],
$\bar{F}_i$ – mean volume marker concentration in the i^{th} grid element [–],
f_r, f_z – radial and axial unit forces [m·s^{-2}],
g – acceleration of gravity [m·s^{-2}],
k – wave number of perturbation ($=2/\lambda$) [m^{-1}],
p – pressure [Pa],
p' – pressure perturbation [Pa],
R – radius of core stream in basic undisturbed flow [m],
Re – Reynolds' number ($=2\bar{w}_B r_2 \rho_B/\mu_B$) [-],
r, z – cylindrical coordinates [m],
r_0 – inner radius of the central dosing pipe [m],
r_1 – outer radius of the central dosing pipe [m],
r_2 – inner radius of the first cylindrical mixer section [m],
S – surface of a deformed inclusion [m^2],
T – time period of instabilities [s],
t – time [s],
W – axial velocity of basic undisturbed flow [m·s^{-1}],
u, w – radial and axial velocity components [m·s^{-1}],
u', w' – radial and axial velocity perturbations [m·s^{-1}],
V_i – volume of the i^{th} grid element [m^3],

v_i – velocity component [m·s^{-1}],
$\bar{w}$ – mean axial velocity [m·s^{-1}],
x, y, z – Cartesian coordinates [m].

Greek letters
α – rate of deformation [s^{-1}],
δ – interface amplitude function [m],
ϕ – amplitude function [m^3·s^{-1}],
λ – wavelength [m],
μ – dynamic viscosity [Pa·s],
v – kinematic viscosity [m^2·s^{-1}],
ρ – density [kg·m^{-3}],
τ_{ij} – components of stress tensor [Pa],
ξ – disturbance of the liquid-liquid interface [m],
Ψ – stream function [m^3·s^{-1}].

Subscripts
A – core (central) stream or inclusion,
B – annular (main) stream or matrix.

Differential operators
$$D \equiv \frac{\partial^2}{\partial r^2} - \frac{1}{r}\frac{\partial}{\partial r} + \frac{\partial^2}{\partial z^2},$$
$$L \equiv \frac{d^2}{dr^2} - \frac{1}{r}\frac{d}{dr}.$$

1. Introduction

When two liquids are mixed in a laminar flow, the process is affected by several factors, *e.g.* the input of mechanical energy, the geometry of a mixer, the volume ratio and the physical properties of the mixed liquids. It is well known that mixing components differing in viscosity is more difficult than in the case of equally viscous liquids [1–3]. Especially mixing on the molecular scale (micromixing) can be retarded [4]. This phenomenon is observed in single-phase systems (with no interfacial tension) [5–7].

Mixing on the molecular scale in the laminar flow is accomplished through molecular diffusion in deformed fluid elements [8, 9]. Viscous deformation generates a new contact surface, decreases segregation scales in the system, and maintains high local concentration gradients. Thus, molecular diffusion can proceed and decrease the concentration variances in the system in a reasonably short time. However, when a small volume of a very viscous liquid is mixed with a less viscous liquid matrix, deformation of elements of the more viscous liquid is very slow and molecular transport of species is not effective. When a small volume of a less viscous liquid is mixed with a more viscous liquid matrix, deformation of the less viscous elements is expected to be at least as fast as deformation in the surrounding liquid. This problem can be illustrated quantitatively by considering an ellipsoidal inclusion of a liquid of viscosity μ_A immersed in a large volume of another liquid of viscosity μ_B, subjected to simple axi-symmetrical elongation (Figure 1):

$$v_x = \alpha_B x/2, \qquad v_y = \alpha_B y/2, \qquad v_z = -\alpha_B z. \tag{1}$$

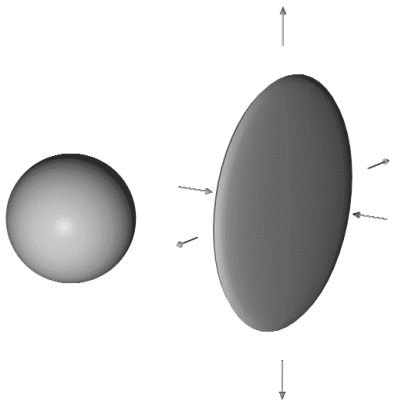

Figure 1. An inclusion deformed in axi-symmetric elongational flow

The flow field within the deformed spot is also linear, but its characteristic rate of deformation, α_A, is different from α_B and depends on the viscosity ratio of the liquids and the shape of the inclusion [10]:

$$\frac{\alpha_A}{\alpha_B}=\left\{1+\left(1-\frac{\mu_A}{\mu_B}\right)\left[1-\left(1-\frac{3a_1^2a_3}{2(a_1^2-a_3^2)^{\frac{3}{2}}}\left(\arccos\left(\frac{a_3}{a_1}\right)-\frac{a_3}{a_1}\left(1-\frac{a_3^2}{a_1^2}\right)^{\frac{1}{2}}\right)\right)\frac{a_1^2+2a_3^2}{a_1^2-a_3^2}\right]\right\}^{-1}. \quad (2)$$

The length of the spot semi-axes can be found from the following equations:

$$\alpha_A=\frac{2}{a_1}\cdot\frac{da_1}{dt}=\frac{2}{a_2}\cdot\frac{da_2}{dt}=-\frac{1}{a_3}\cdot\frac{da_3}{dt}. \quad (3)$$

Figure 2 shows how the viscosity ratio affects the generation of a new contact area between the mixed liquids. When the inclusion is more viscous than its environment ($\mu_A>\mu_B$), mixing is very slow, and this explains why it is so often difficult to achieve homogenisation in this case. When the inclusion is less viscous than the environment ($\mu_A<\mu_B$), a new contact surface is created faster, but the viscosity effect is rather small and limited in time.

Figure 2 shows that deformation of the less viscous inclusion is accelerated only at the beginning of the process, provided that the rate of deformation is kept constant (which is very difficult to achieve in real industrial mixers). Liquid elements are usually subjected to a rate of deformation strongly varying in time and space. This, in the presence of an interfacial tension and/or large difference in viscosities of the two mixed fluids at their interface, creates favourable conditions for flow destabilisation to occur. In two-phase systems, destabilisation results in the formation of smaller drops of the dispersed material until the interfacial tension retards further dispersion [2, 4]. When the mixed liquids are fully miscible, the spot or thread formed by the less viscous liquid may begin to oscillate. This may be followed by irregular destabilisation or the oscillations may die due to the external elongational flow field [6]. During such oscillations, periodic structures are formed, *e.g.* a line of ellipsoids. New intermaterial surface is constantly created and destroyed in each oscillation cycle. Under such conditions, micromixing may be significantly retarded [4].

The aim of this work is to model the process of formation of the periodic structures observed in experiments, and predicted by the theory of hydrodynamic

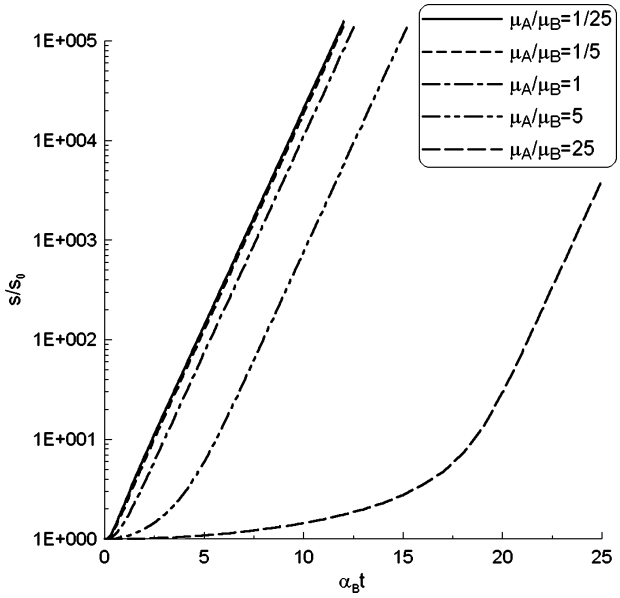

Figure 2. Growth of the material surface of an inclusion deformed in elongational flow

stability, by means of Computational Fluid Mechanics (CFD). The numerical methods used in the flow simulations are the finite-element method and the volume of fluid method (VOF), which has already been used for this purpose for two-phase systems [11, 12].

The investigated flow is an axi-symmetric, core-annular flow in a straight, vertical and circular tube of varying cross-section. Both liquids are Newtonian and have different viscosity and density. Sizes and time periods of the experimentally observed instabilities of the core stream are compared with sizes and time periods of the instabilities simulated numerically and determined by the stability analysis.

2. Experimental

Mixing of two liquid streams of different viscosity and density was conducted in an on-line perspex mixer shown in Figure 3. The upper and lower sections of the mixer are cylindrical, while the middle section is a cone-shaped nozzle. A syringe pump was used to feed the central liquid stream into the mixer via a small cooper pipe positioned at the mixer axis. The main stream was fed into the mixer from a pressurised container located above the mixer.

The central stream contained iodine and the main stream contained sodium thiosulfate. The substrates were consumed in a decolourisation reaction, which helped to visualise the front of mixing. Starch syrup was used to regulate viscosity of the aqueous reactant solutions, while density of the mixed solutions was adjusted by the addition of potassium iodide. The experiments were recorded by means of a video camera.

Figure 4 shows three distinct patterns of the core-annular flow observed in the mixer. The first pattern (Figure 4a) is observed when both solutions have the same viscosity. The central stream is slowed down behind the tip of the feeding pipe and

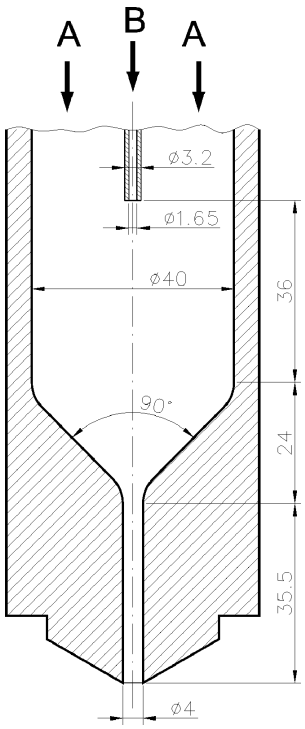

Figure 3. Scheme of the experimental system: A – iodine solution (core stream), B – sodium thiosulfate solution (annular stream)

its diameter rapidly increases. The extensional flow in the mixer nozzle decreases the stream cross-section again. The second flow pattern (Figure 4b) is observed when the central stream is more viscous than the main stream. In this case, stability of the central stream is hardly affected by the external flow. The third flow pattern (Figure 4c) is observed when the central stream is less viscous than the main stream. Unlike the first two patterns, the flow is unstable and the central stream forms a line of ellipsoids, which emerge from the tip of the feeding pipe. The ellipsoids are transported down stream to the mixer nozzle, where oscillations are destroyed by extensional flow. However, the instabilities may re-emerge in the cylindrical outlet.

It should be noted that no break-up of a destabilised central stream has ever been observed, which is due to the lack of interfacial tension between the mixed liquids. The size of the swellings and the frequency of their generation depend mainly on the feeding rate of the central stream, viscosity and density of the liquids. At very low feeding rates, destabilisation does not occur unless forced by an external mechanical impulse. At very high feeding rates, the observed destabilisation is asymmetric and irregular.

3. Numerical simulation of flow destabilisation

Destabilisation of the core-annular flow was modelled by numerical integration of the equations of continuity and momentum conservation. Computations were conducted under the following assumptions:

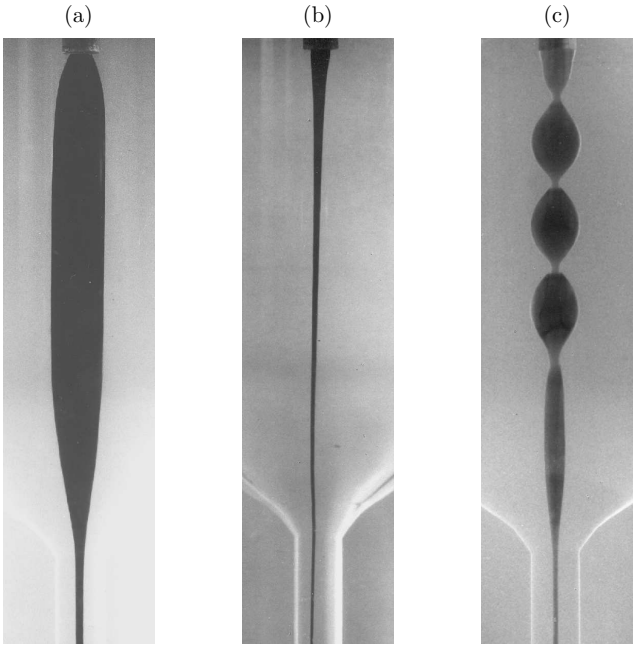

Figure 4. Typical patterns of core-annular flow:
(a) liquids of equal viscosity ($\bar{w}_A/\bar{w}_B = 26.2$, $\mathrm{Re} = 9.1$);
(b) more viscous liquid in the core ($\bar{w}_A/\bar{w}_B = 19.8$, $\mu_A/\mu_B = 128$);
(c) less viscous liquid in the core ($\bar{w}_A/\bar{w}_B = 24.2$, $\mu_A/\mu_B = 0.00236$)

a) the flow is laminar, axi-symmetric and isothermal,
b) the mixed liquids are Newtonian, incompressible and fully miscible.

The assumption that the flow is axi-symmetric is justified by the experimental evidence indicating that, as long as the flow destabilisation is regular, the axial symmetry is maintained in the mixer. In such a case, the governing equations written in cylindrical coordinates read as follows:

a) the equation of continuity

$$\frac{\partial \rho}{\partial t} + \frac{1}{r}\frac{\partial (\rho r u)}{\partial r} + \frac{\partial (\rho w)}{\partial z} = 0, \tag{4}$$

b) the equations of momentum conservation

$$\rho\left(\frac{\partial u}{\partial t} + u\frac{\partial u}{\partial r} + w\frac{\partial u}{\partial z}\right) = \rho f_r - \frac{\partial p}{\partial r} + \frac{1}{r}\frac{\partial (r\tau_{rr})}{\partial r} + \frac{\partial \tau_{rz}}{\partial z}, \tag{5}$$

$$\rho\left(\frac{\partial w}{\partial t} + u\frac{\partial w}{\partial r} + w\frac{\partial w}{\partial z}\right) = \rho f_r - \frac{\partial p}{\partial z} + \frac{1}{r}\frac{\partial (r\tau_{rz})}{\partial r} + \frac{\partial \tau_{zz}}{\partial z}. \tag{6}$$

The components of the viscous stress tensor are given by:

$$\tau_{rr} = 2\mu\frac{\partial u}{\partial r}, \qquad \tau_{rz} = \tau_{zr} = \mu\left(\frac{\partial u}{\partial z} + \frac{\partial w}{\partial r}\right), \qquad \tau_{zz} = 2\mu\frac{\partial w}{\partial z}. \tag{7}$$

Galerkin's finite-element method is used to solve the system of Equations (4)–(7) with the following boundary conditions:

a) at the mixer walls $u, w = 0$,

b) at the mixer axis and inlet sections $u=0$,
c) at the central inlet $w=2\bar{w}_A[1-(r/r_0)^2]$,
d) at the annular inlet

$$w=2\bar{w}_B\left[1-\left(\frac{r}{r_2}\right)^2+\frac{1-(r_1/r_2)^2}{\ln(r_2/r_1)}\ln(r/r_2)\right]\Bigg/\left[1+\left(\frac{r_1}{r_2}\right)^2-\frac{1-(r_1/r_2)^2}{\ln(r_2/r_1)}\right]. \quad (8)$$

The volume occupied by the centrally injected liquid is tracked to determine a new liquid-liquid interface. Then, the finite-element method is used to update the velocity field, and this computation scheme is applied at each time step. An inert marker represents the tracked fluid volume. Marker concentration F equals 1 within the tracked volume and 0 outside this volume. Steep gradients in tracer concentration represent the interface position. The transport equation for the volume marker reads [11, 12]:

$$\frac{\partial F}{\partial t}+u\frac{\partial F}{\partial r}+w\frac{\partial F}{\partial z}=0. \quad (9)$$

The fractional fill of a grid element of given volume V_i is defined as:

$$\bar{F}_i=\frac{1}{V_i}\int_{V_i}F dV_i. \quad (10)$$

Viscosity and other physical properties of the liquids depend on the fractional fill:

$$\mu=\bar{F}_i\mu_A+(1-\bar{F}_i)\mu_B. \quad (11)$$

It is assumed that initially the tracked volume occupies only the small central pipe. As fresh liquid is constantly fed into the pipe, the tracked volume grows and spreads along the mixer axis as shown in Figure 5.

Figure 5. Subsequent stages of simulation of unstable core-annular flow; $\bar{w}_A/\bar{w}_B=21.6$, $\mathrm{Re}=0.106$, $\mu_A/\mu_B=0.00231$, $\rho_A/\rho_B=1.023$

The numerical simulations were conducted with the Fluent Dynamics Analysis Package, FIDAP 7.6. A computational grid consisting of quadrilateral elements was

constructed using the GAMBIT 1.3 mesh generator. Element size in the central region of the mixer, where flow destabilisation occurs, was set to 0.005 of the overall mixer diameter. When element size was larger than 0.075, it was impossible to correctly simulate destabilisation. When the element size was smaller than 0.005, computation times were very long and predicted destabilisation was irregular, probably due to accumulations of round-off errors. All computations were done on a Compaq DS 20 workstation equipped with two 500MHz processors and 1.2GBRAM. The destabilised core-annular flow was simulated only in the cylindrical section of the mixer.

4. Linear stability analysis

Another method used to investigate stability of the core-annular flow is based on the linear theory of hydrodynamic stability [13, 14]. This method allows one to check whether the flow is potentially unstable, *e.g.* if infinitely small perturbations of the liquid-liquid interface can grow and destabilise the basic flow (see Figure 6). Non-linear phenomena and the effect of the varying deformation rate on flow stability cannot be accounted for, but the method still allows one to determine the size (wavelength) and time period of the instabilities. Therefore, it can be very interesting to compare the results of linear stability analysis with the results of experiments and direct numerical simulation.

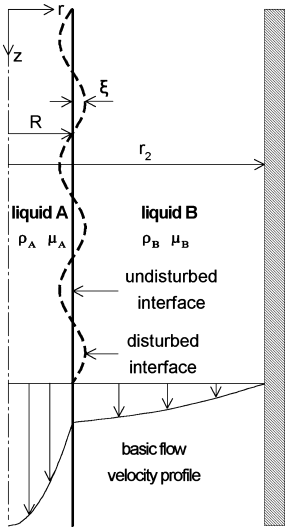

Figure 6. Sketch of core-annular flow

Assuming that the basic core-annular flow is axi-symmetric and caused by two forces, namely the pressure gradient and the earth's gravity acting along the system axis, the particular solution of governing Equations (4)–(7) reads thus:

$$0 \le r \le R \quad W(r) = \left(\rho_A g - \frac{\partial P}{\partial z}\right) \frac{R^2 - r^2}{4\mu_A} +$$

$$+\left(\rho_B g-\frac{\partial P}{\partial z}\right)\frac{r_2^2-R^2}{4\mu_B}-\frac{\rho_A-\rho_B}{2\mu_B}gR^2\ln\left(\frac{R}{r_2}\right), \tag{12}$$

$$R\le r\le r_2 \quad W(r)=\left(\rho_B g-\frac{\partial P}{\partial z}\right)\frac{r_2^2-r^2}{4\mu_B}-\frac{\rho_A-\rho_B}{2\mu_B}gR^2\ln\left(\frac{r}{r_2}\right). \tag{13}$$

Perturbations of the basic flow can be taken into account as follows:

$$u=u', \qquad w=W+w', \qquad p=P+p'. \tag{14}$$

Introduction of Equation (14) and the basic solution (12)–(13) into the governing Equations (4)–(7), while neglecting non-linear perturbation terms, gives:

$$\frac{1}{r}\frac{\partial(ru')}{\partial r}+\frac{\partial w'}{\partial z}=0, \tag{15}$$

$$\rho\left(\frac{\partial u'}{\partial t}+W\frac{\partial u'}{\partial z}\right)=-\frac{\partial p'}{\partial r}+\mu\left[\frac{\partial}{\partial r}\left(\frac{1}{r}\frac{\partial(ru')}{\partial r}\right)+\frac{\partial^2 u'}{\partial z^2}\right], \tag{16}$$

$$\rho\left(\frac{\partial w'}{\partial t}+u'\frac{\partial W}{\partial r}+W\frac{\partial w'}{\partial z}\right)=-\frac{\partial p'}{\partial z}+\mu\left[\frac{1}{r}\frac{\partial}{\partial r}\left(r\frac{\partial w'}{\partial r}\right)+\frac{\partial^2 w'}{\partial z^2}\right]. \tag{17}$$

Similarly to direct numerical simulations, it is assumed that the perturbed flow is axisymmetric, which allows velocity components to be expressed in terms of the Stokes stream function [13]:

$$u'=\frac{1}{r}\frac{\partial\Psi}{\partial z}, \qquad w'=-\frac{1}{r}\frac{\partial\Psi}{\partial r}. \tag{18}$$

Thus, the continuity Equation (15) is automatically fulfilled, while the momentum Equations (16)–(17) can be reduced to a single equation:

$$\left(\frac{\partial}{\partial t}+W\frac{\partial}{\partial z}\right)\cdot D\Psi-\frac{\partial\Psi}{\partial z}\cdot r\frac{\partial}{\partial r}\left(\frac{1}{r}\frac{\partial W}{\partial r}\right)=v\cdot D(D\Psi). \tag{19}$$

The stream function of the perturbed flow has the following form [13]:

$$\Psi(r,z,t)=\phi(r)\cdot\exp[ik(z-ct)]. \tag{20}$$

Introduction of Equation (20) into Equation (19) yields the well-known Orr-Sommerfeld equation:

$$(W-c)(L-k^2)\phi-r\phi\frac{d}{dr}\left(\frac{1}{r}\frac{dW}{dr}\right)=\frac{v}{ik}(L-k^2)^2\phi. \tag{21}$$

The system of one such equation for the central stream and another for the annular stream should be supplemented with appropriate boundary conditions:

- u'_A, w'_A, p'_A are finite at the system axis,
- $u'_B=w'_B=0$ at the system wall,
- and

$$u'_A=u'_B, \qquad W_A+w'_A=W_B+w'_B, \tag{22}$$

$$(\tau'_{zr})_A-(\tau'_{zr})_B=(\rho_A-\rho_B)g\xi, \qquad (-p'+\tau'_{rr})_A-(-p'+\tau'_{rr})_B=0. \tag{23}$$

at the liquid-liquid interface [14].

The disturbance of the liquid-liquid interface present in the boundary conditions

$$\xi(r,z,t) = \delta(r) \cdot \exp[ik \cdot (z - ct)] \tag{24}$$

is related to the velocity field as follows [14]:

$$u' = \frac{\partial \xi}{\partial t} + W \frac{\partial \xi}{\partial z}. \tag{25}$$

Approximating the amplitude functions, $\phi(r)$, by the finite series of modified Chebyshev polynomials:

$$\phi_A(r) = \frac{D_0}{2} T_0^*(\tilde{x}) + \sum_{i=1}^{M} D_i T_i^*(\tilde{x}), \qquad \tilde{x} = \frac{r}{R}, \tag{26}$$

$$\phi_B(r) = \frac{C_0}{2} T_0^*(\tilde{y}) + \sum_{i=1}^{N} C_i T_i^*(\tilde{y}), \qquad \tilde{y} = \frac{r - R}{r_2 - R}, \tag{27}$$

transforms the system of two Orr-Sommerfeld Equations (21) and the associated boundary conditions (22)–(23) into a general eigenvalue problem for an imaginary wave speed c:

$$\bar{\bar{A}} \cdot \vec{V} = c \cdot \bar{\bar{B}} \cdot \vec{V}. \tag{28}$$

Matrices $\bar{\bar{A}}$ and $\bar{\bar{B}}$ are related to the wave number, the flow conditions and the liquid properites. $\vec{V}$ is the vector of coefficients C_i and D_i. The method of finding eigenvalues of Equation (28) applied here has been described earlier [6, 15].

When the eigenvalue is found with the negative imaginary part, $\mathrm{Im}(c)$, it means that the flow is potentially unstable. In this case, the amplitude of perturbations increases exponentially with time, and it is assumed that the fastest growing disturbance becomes the dominant one [13, 14]. The characteristic wavelength of such perturbation corresponds to the global maximum of the growth rate of the disturbance (Figure 7).

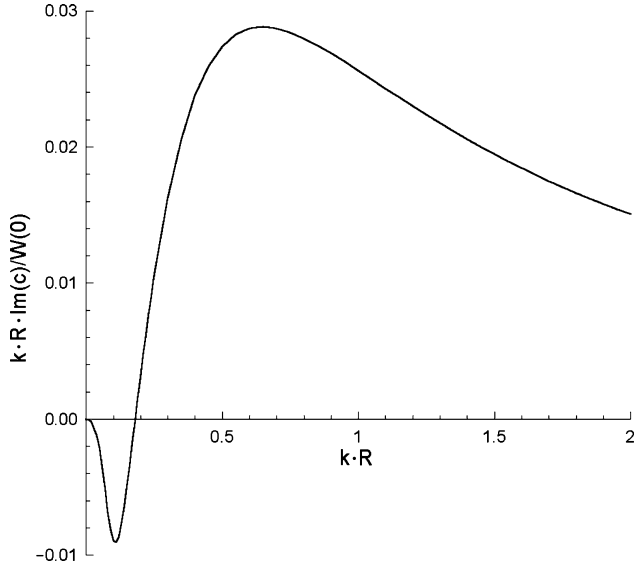

Figure 7. The growth rate of disturbances in core-annular flow; $\bar{w}_A/\bar{w}_B = 21.6$, $\mathrm{Re} = 0.106$, $\mu_A/\mu_B = 0.00231$, $\rho_A/\rho_B = 1.023$

The real part of the eigenvalue, $\mathrm{Re}(c)$, can be used to calculate the characteristic time period of the instabilities:

$$T = \lambda / \mathrm{Re}(c). \tag{29}$$

Finally, it should be noted that in the analysed case (a single-phase system) flow destabilisation is caused solely by the discontinuity of viscosity and density at the liquid-liquid interface. In practice there are large gradients of these properties. In a two-phase system, a non-zero interfacial tension is an additional and often a dominant source of flow instability.

5. Results and discussion

The direct flow simulations and stability calculations were carried out for two series of experiments in which instabilities were observed in a wide range of flow rates of the central stream. In both series of experiments, the central (core) stream was approximately 400 time less viscous than the main (annular) stream. However, in the first series of experiments the liquids' densities differed only slightly, whereas in the second series the core liquid density was 12% higher than density of the annular stream, and consequently the flow was potentially more susceptible to destabilisation. Table 1 shows the physical properties of liquids used in the experiments.

Table 1. Density and viscosity of liquids used in the experiments

Experiments	First series		Second series	
streams	core	annular	core	annular
ρ [kg·m^{-3}]	1359	1328	1492	1328
μ [Pa·s]	0.001	0.433	0.001	0.414

Figure 8 shows two pictures shot during the first series of experiments for different flow rates of the central stream. Accompanying these pictures, there are plots based on the numerical data obtained by means of computational fluid dynamics (CFD) and showed in the same scale. It can be seen that the volume of fluid method (VOF) is capable of simulating destabilisation of the core-annular flow. It should be noted, however, that the sizes of ellipsoids of the central stream predicted by CFD are smaller than those determined experimentally.

The stability theory also predicts wavelengths of the instabilities smaller than those determined experimentally (see Table 2). At the same time, the characteristic time period of the instabilities observed in the experiments is shorter than that obtained by the CFD method, but longer than the one determined by the stability theory (see Table 3).

For very small flow rates of the central stream, the CFD-based model was unable to predict flow destabilisation.

Figure 9 and Tables 4 and 5 show results obtained for the second series of tests. In this case, the flow is potentially more unstable due to greater difference in density between the core and the annular streams, and the CFD method is capable to model flow destabilisation for flow rates of the central stream smaller than in the first series of experiments.

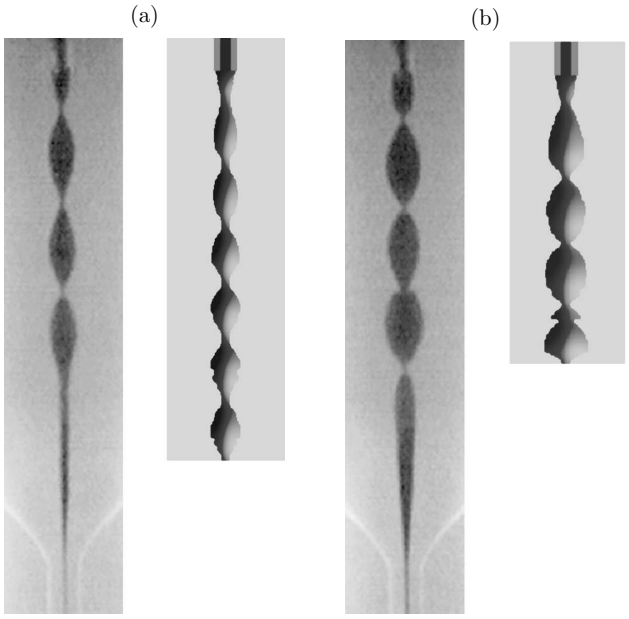

Figure 8. Comparison of experimental visualisation with CFD modelling, the first series of experiments; $\mu_A/\mu_B = 0.00231$, $\rho_C/\rho_D = 1.023$: (a) $\bar{w}_A/\bar{w}_B = 21.6$, Re = 0.106; (b) $\bar{w}_A/\bar{w}_B = 42.1$, Re = 0.109

Table 2. Wavelength of instabilities determined for the first series of experiments

Re	$\bar{w}_A/\bar{w}_B$	Experiment		CFD model		Stability theory [mm]
		first swelling [mm]	second swelling [mm]	first swelling [mm]	second swelling [mm]	
0.107	10.7	8.3	7.8	—	—	6.5
0.106	21.6	11.0	10.2	7.7	7.6	7.7
0.109	42.1	10.2	10.0	8.6	7.7	8.6
0.112	54.6	9.3	10.5	8.5	9.2	8.4

Table 3. Time period of instabilities determined for the first series of experiments

Re	$\bar{w}_A/\bar{w}_B$	Experiment [s]	CFD model [s]	Stability theory [s]
0.107	10.7	2.03	—	1.87
0.106	21.6	1.93	2.16	1.67
0.109	42.1	1.67	1.90	1.35
0.112	54.6	1.53	1.79	1.25

In all the analysed situations, a regular destabilisation of the central stream, when predicted by CFD (FIDAP 7.6), is limited to 4 or, at most, 6 ellipsoids, most probably due to an accumulation of the round-off errors in the computations. The general rule is that for higher flow rates of the central stream the predicted instability becomes more irregular. The same phenomenon is observed in experiments, but then irregular destabilisation occurs at higher flow rates.

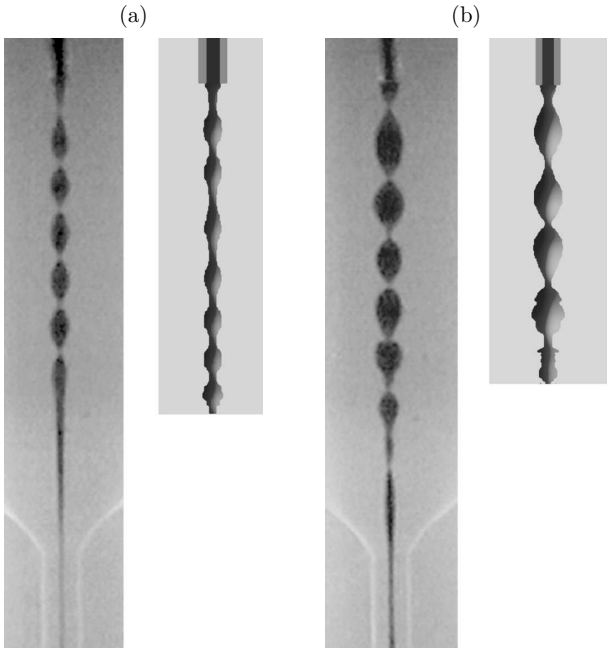

Figure 9. Comparison of experimental visualisation with CFD modelling, the second series of experiments; $\mu_A/\mu_B = 0.00242$, $\rho_A/\rho_B = 1.12$: (a) $\bar{w}_A/\bar{w}_B = 10.8$, Re = 0.111; (b) $\bar{w}_A/\bar{w}_B = 41.8$, Re = 0.115

Table 4. Wavelength of instabilities determined for the second series of experiments

Re	$\bar{w}_A/\bar{w}_B$	Experiment		CFD model		Stability theory [mm]
		first swelling [mm]	second swelling [mm]	first swelling [mm]	second swelling [mm]	
0.111	5.4	5.1	5.1	—	—	3.6
0.111	10.8	6.1	5.9	5.2	5.2	4.3
0.112	21.5	7.2	6.4	6.2	6.0	4.8
0.115	41.8	8.7	6.9	7.6	7.8	4.6

Table 5. Time period of instabilities determined for the second series of experiments

Re	$\bar{w}_A/\bar{w}_B$	Experiment [s]	CFD model [s]	Stability theory [s]
0.111	5.4	0.83	—	0.75
0.111	10.8	0.74	0.95	0.63
0.112	21.5	0.64	0.76	0.48
0.115	41.8	0.62	0.72	0.38

6. Conclusions

The destabilisation of the core-annular flow of two liquids differing in viscosity and density has been studied both experimentally and theoretically.

The experiments showed that when the liquid in the core was less viscous than the surrounding liquid, the flow became unstable. The core stream formed a line of

ellipsoids instead of a straight cylindrical thread, as in other cases when the contacted liquids were equally viscous or the core liquid was more viscous than the surrounding liquid. The observed phenomenon has significant consequences in laminar micromixing of liquids differing in viscosity: when flow destabilisation occurs, periodic segregated structures can be formed and molecular diffusion cannot be efficiently accelerated by mechanical mixing.

Two theoretical methods were used to model the observed flow destabilisation: numerical flow simulation (the CFD model) and the theory of hydrodynamic stability. The first model was based on a direct integration of the mass and momentum conservation equations using the finite-element approach. To track the "minor" component of different viscosity and density than the "major" component, the volume of fluid method was applied. Flow destabilisation was predicted in most cases, except for situations when the computation grid was too coarse to correctly model the flow in a very thin core stream. The wavelength and the characteristic time periods of the instabilities obtained in the computations were close to the values determined experimentally. These results were also positively verified against the theory of hydrodynamic stability, *i.e.* the second model used in the present work. This shows that the applied CFD method can be useful in a further study of the complicated process of mixing liquids of differing viscosity and density.

Acknowledgements

This work was supported financially by the Polish State Committee for Scientific Research (KBN) under grant No 7 T09C 056 21.

References

[1] Tomotika S 1936 *Proc. Roy. Soc. London* **A 153** 302
[2] Grace H P 1981 *Chem. Engng. Commun.* **14** 225
[3] Bouwmans I, Bakker A and van den Akker H E A 1997 *Trans. IchemE* **75** 777
[4] Ranz W E 1982 *AIChE Journal* **28** 91
[5] Murakami Y, Fujimoto K and Uotani S 1972 *J. Chem. Engng. Japan* **5** 85
[6] Bałdyga J and Rożeń A 1994 *Proc. 8th European Conf. Mixing*, Cambridge, England, pp. 267–274
[7] Rożeń A, Bakker R A and Bałdyga J 2000 *Proc. 10th European Conf. Mixing*, Delft, The Netherlands, pp. 85–92
[8] Ottino J M, Ranz W E and Macosko C W 1979 *Chem. Engng. Sci.* **34** 877
[9] Rożeń A, Bakker R A and Bałdyga J 2001 *Chem. Engng. J.* **84** 413
[10] Eshelby J D 1957 *Proc. Roy. Soc. London* **A 241** 376
[11] Zhang X 1999 *Chem. Engng. Sci.* **54** 1759
[12] Li J, Renardy Y Y and Renardy M 2000 *Phys. Fluids* **12** 269
[13] Drazin P G and Reid W H 1981 *Hydrodynamic Stability*, Cambridge University Press
[14] Joseph D D and Renardy Y Y 1993 *Fundamentals of Two-fluid Dynamics*, Springer-Verlag
[15] Rożeń A 1995 *Investigation of Micromixing in Viscous Liquids*, PhD Thesis, Warsaw University of Technology, Poland